Optimum Operating Conditions for Subcritical/Supercritical Fluid-Based Natural Circulation Loops

Ajay Kumar Yadav
Assistant Professor
Department of Mechanical Engineering,
National Institute of Technology,
Karnataka, Surathkal,
Mangalore 575025, Karnataka, India
e-mail: ajaykyadav@nitk.edu.in

Souvik Bhattacharyya[1]
Professor
Department of Mechanical Engineering,
Indian Institute of Technology Kharagpur,
Kharagpur 721302, India
e-mail: souvik.iit@gmail.com

M. Ram Gopal
Professor
Department of Mechanical Engineering,
Indian Institute of Technology Kharagpur,
Kharagpur 721302, India
e-mail: ramg@mech.iitkgp.ernet.in

Natural circulation loop (NCL) is simple and reliable due to the absence of moving components and is preferred in applications where safety is of foremost concern, such as nuclear power plants and high-pressure thermal power plants. In the present study, optimum operating conditions based on the maximum heat transfer rate in NCLs have been obtained for subcritical as well as supercritical fluids. In recent years, there is a growing interest in the use of carbon dioxide (CO_2) as loop fluid in NCLs for a variety of heat transfer applications due to its excellent thermophysical environmentally benign properties. In the present study, three-dimensional (3D) computational fluid dynamics (CFD) analysis of a CO_2-based NCL with isothermal source and sink has been carried out. Results show that the heat transfer rate is much higher in the case of supercritical phase (if operated near pseudocritical region) than the subcritical phase. In the subcritical option, higher heat transfer rate is obtained in the case of liquid operated near saturation condition. Correlations for optimum operating condition are obtained for a supercritical CO_2-based NCL in terms of reduced temperature and reduced pressure so that they can be employed for a wide variety of fluids operating in supercritical region. Correlations are also validated with different loop fluids. These results are expected to help design superior optimal NCLs for critical applications. [DOI: 10.1115/1.4031921]

Keywords: heat transfer, natural circulation loops, carbon dioxide, supercritical fluid, pseudocritical point

1 Introduction

Since NCLs work on buoyancy effect caused by density gradient, no moving components, such as pumps and compressors, are required to circulate the loop fluid. Such simple and reliable characteristics of NCLs attract various engineering applications particularly in small to medium capacity systems and are always preferred where safety is of foremost concern irrespective of plant capacity. NCLs are widely used in applications, such as refrigeration and air conditioning systems, solar collectors, nuclear reactors, high-pressure power plant, and transformer cooling. Since performance of the loop directly depends on the loop fluids, selection of loop fluids plays a vital role. In recent years, CO_2 has emerged as a preferred loop fluid [1–3] due to its favorable thermophysical properties in addition to its environmental benignity (zero *ozone depletion potential* and negligible *global warming potential*). The studies show that for low-temperature refrigeration and air conditioning applications, CO_2-based NCLs are more compact in comparison to other conventional working fluids [2] and have been proposed for various heat transfer applications, such as geothermal [4–6], solar collector [7], stirling cooler [8], and heat pump [9,10]. In a recent review paper by Sarkar et al. [11] on supercritical NCLs for nuclear applications, it was indicated that CO_2 as a working fluid leads to higher flow and hence greater heat transfer rates compared to water, thereby making it the superior working fluid.

The studies carried out by Yadav et al. [12] for the subcritical region of liquid CO_2-based NCLs show that the best operating condition for maximum heat transfer rate is found near the saturation pressure for the required temperature. Since the critical temperature of CO_2 is low (≈31 °C), it becomes necessary to operate the loop with CO_2 in supercritical region when the temperatures of the heat source and sink are high. A large number of studies, on heat transfer in the supercritical region using different fluids for both forced as well as NCLs, show that higher heat transfer rates are obtained when the fluids are operated near what is called the pseudocritical point [13–18].

In general, pseudocritical point is defined as the temperature at which the specific heat (c_p) of fluid at constant pressure reaches a maximum value [19–22]. For NCLs, the volumetric expansion coefficient plays an important role. At a given pressure, the property variation with temperature shows that the volumetric expansion coefficient reaches its maximum value at a temperature, which is not exactly the same as the temperature at which c_p becomes the maximum. It is well known that near pseudocritical region, other thermophysical properties relevant in NCLs also vary abruptly. Hence, it will be more meaningful to define optimum operating condition for natural convection based on Rayleigh number which takes care of variation of all the relevant thermophysical properties. Many authors have defined modified Grashof number for the heat transfer studies of NCLs. Based on modified Grashof number, modified Rayleigh number may also be defined. In the present study, three different correlations have been developed based on maximum specific heat (also called pseudocritical point), Rayleigh number, and modified Rayleigh number (Ra_m) for optimum operating condition in supercritical region. It would be convenient if one can obtain the optimum operating condition for a given operating temperature using a general correlation applicable to all fluids operating in the supercritical region. In this study, correlations have been proposed to find the optimum operating condition for different temperatures in the form of reduced parameters.

[1]Corresponding author.

Contributed by the Heat Transfer Division of ASME for publication in the Journal of Heat Transfer. Manuscript received August 2, 2014; final manuscript received September 18, 2015; published online June 14, 2016. Assoc. Editor: Ali Khounsary.

2 Physical Model and Mathematical Formulations

2.1 Physical Model. Figure 1 shows the schematic of 3D rectangular NCL which consists of an isothermal sink, an isothermal source, and left and right insulated pipes. The loop fluid is heated sensibly in the isothermal heat source (T_H) and is cooled sensibly in the isothermal heat sink (T_C). Wall temperatures (T_H and T_C) of source and sink are kept constant. Circulation of the loop fluid is maintained due to the buoyancy effect caused by heating at the bottom and cooling at the top. Geometric and material specifications of the model are given in Table 1.

The following simplifying assumptions are made in the analysis:

(i) The loop fluid, CO_2, is in single-phase throughout the loop.
(ii) The system is operating at steady-state.
(iii) All external walls except the heat source and sink are perfectly insulated.
(iv) Wall material is isotropic with constant thermal conductivity.

2.2 Mathematical Formulations and Solution. The governing mass, momentum, and energy equations are shown below. These equations with relevant boundary conditions are solved by ANSYS (FLUENT) 14.5.

Conservation of mass

$$\nabla \cdot (\rho \mathbf{V}) = 0 \tag{1}$$

Conservation of momentum (Navier–Stokes equation) is expressed as

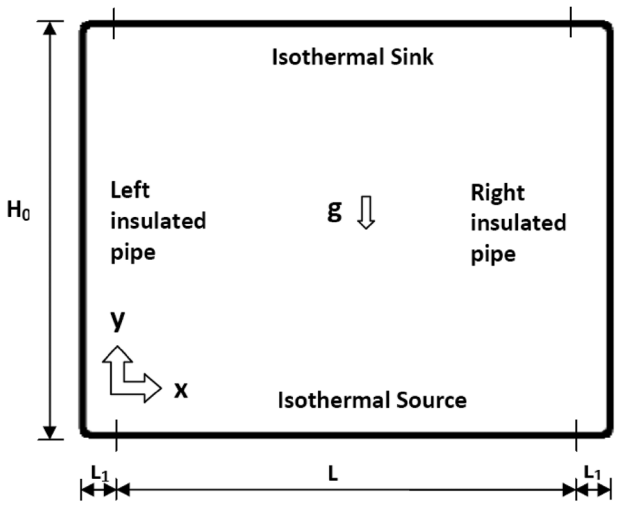

Fig. 1 Schematic of the NCL employed in the model

Table 1 Geometric and material specifications for the model

Parameters	Value
Internal diameter of the loop (d)	15 mm
Length of isothermal sink or source (L)	120 cm
Total width of the loop (L_0)	146 cm
Total height of the loop (H_0)	124.5 cm
Total length of the loop (L_t)	545 cm
Insulated pipe length in horizontal pipe ($2L_1$)	26 cm
Radius of curvature for bend (R)	30 mm
Tube wall thickness	2 mm
Material of the loop	Copper

$$\nabla \cdot (\rho \mathbf{V}\mathbf{V}) = -\nabla p + \nabla \cdot (\bar{\bar{\tau}}) + \rho \mathbf{g} \tag{2}$$

where the stress tensor can be written as

$$\bar{\bar{\tau}} = \mu \left[(\nabla \mathbf{V} + \nabla \mathbf{V}^{\mathrm{T}}) - \frac{2}{3} \nabla \cdot \mathbf{V} I \right]$$

Second term in stress tensor is the effect of volume dilation and I is the unit tensor.

Conservation of energy with viscous dissipation may be expressed as

$$\nabla \cdot (\mathbf{V}(\rho E + p)) = \nabla \cdot (\lambda_{\mathrm{eff}} \nabla T + \bar{\bar{\tau}} \cdot \mathbf{V}) \tag{3}$$

where

$$E = \int_{T_{\mathrm{ref}}}^{T} c_p dT + \frac{V^2}{2} \tag{4}$$

and $T_{\mathrm{ref}} = 298.15$ K.

2.2.1 Model for Turbulence Analysis. Turbulent flow models for supercritical fluids are less developed and still under intense study [23]. In view of that, a general renormalization group (RNG) k–ε model is selected as the first step to introduce the expression of turbulent effect. This method has also been used successfully in previous studies on supercritical CO_2 turbulent flow yielding accurate results [12,18,24].

The transport equations for RNG k–ε model are written as

$$\frac{\partial}{\partial x_i}(\rho k u_i) = \frac{\partial}{\partial x_j}\left(\alpha_k \mu_{\mathrm{eff}} \frac{\partial k}{\partial x_j} \right) + G_k + G_b - \rho \varepsilon \tag{5}$$

$$\frac{\partial}{\partial x_i}(\rho \varepsilon u_i) = \frac{\partial}{\partial x_j}\left(\alpha_\varepsilon \mu_{\mathrm{eff}} \frac{\partial \varepsilon}{\partial x_j} \right) + C_{1\varepsilon} \frac{\varepsilon}{k}(G_k + C_{3\varepsilon} G_b) - C_{2\varepsilon} \rho \frac{\varepsilon^2}{k} - R_\varepsilon \tag{6}$$

where G_k and G_b are the generation of turbulence kinetic energy due to the mean velocity gradients and buoyancy, respectively,

$$G_k = \mu_t S^2 \tag{7}$$

where S is the modulus of the mean rate-of-strain tensor, defined as

$$S \equiv \sqrt{2 S_{ij} S_{ij}} \tag{8}$$

S_{ij} is the rate-of-strain tensor defined as

$$S_{ij} \equiv \frac{1}{2}\left(\frac{\partial u_i}{\partial x_i} + \frac{\partial u_j}{\partial x_i} \right) \tag{9}$$

$$\mu_t = \rho C_\mu k^2 / \varepsilon \tag{10}$$

Generation of turbulence due to buoyancy is given by

$$G_b = \beta g_i \frac{\mu_t}{\mathrm{Pr}_t} \frac{\partial T}{\partial x_i} \tag{11}$$

where

$$\beta = -\frac{1}{\rho}\left(\frac{\partial \rho}{\partial T} \right)_p \tag{12}$$

$$\mathrm{Pr}_t = 1/\alpha \tag{13}$$

$$\left|\frac{\alpha-1.3929}{\alpha_0-1.3929}\right|^{0.6321}\left|\frac{\alpha+2.3929}{\alpha_0+2.3929}\right|^{0.3679}=\frac{\mu}{\mu_{\text{eff}}} \tag{14}$$

$$\alpha_0=1/\text{Pr}=\lambda/\mu c_\text{p} \tag{15}$$

$$R_\varepsilon=\frac{C_\mu\rho\eta^3(1-\eta/\eta_0)\varepsilon^2}{(1+0.012\eta^3)k} \tag{16}$$

where $\eta\equiv Sk/\varepsilon$, $\eta_0=4.38$, $C_\mu=0.0845$, $\alpha_k=\alpha_\varepsilon=1.393$, $C_{1\varepsilon}=1.42$, and $C_{2\varepsilon}=1.68$

$$C_{3\varepsilon}=\tan h\left|\frac{v}{u}\right| \tag{17}$$

where v is the component of the flow velocity parallel to the gravitational vector and u is the component of the flow velocity perpendicular to the gravitational vector.

Equation for the effective viscosity is given by

$$d\left(\frac{\rho^2k}{\sqrt{\varepsilon\mu}}\right)=1.72\frac{\hat{v}}{\sqrt{\hat{v}^3-1+C_v}}d\hat{v} \tag{18}$$

where

$$\hat{v}=\mu_{\text{eff}}/\mu \tag{19}$$

and $C_v\approx 100$.

Effective conductivity is expresses as

$$\lambda_{\text{eff}}=\alpha C_\text{p}\mu_{\text{eff}} \tag{20}$$

The following terms are defined to describe the fluid flow and heat transfer phenomena.

Mass flow rate at any cross section is defined as

$$m=\int_0^A\rho V dA \tag{21}$$

Local bulk mean temperature of the fluid is expressed as

$$T=\frac{\int_0^A c_\text{p}T\rho V dA}{\int_0^A c_\text{p}\rho V dA} \tag{22}$$

Steady-state Reynolds number and modified Grashof number [25] are defined as

$$\text{Re}=\frac{4m}{\pi d\mu} \tag{23}$$

$$\text{Gr}_\text{m}=\frac{g\beta d^3\rho^2QH_0}{A\mu^3c_\text{p}} \tag{24}$$

where Q is the heat transfer rate from the heat source to the sink.

Heat transfer rate at source/sink wall

$$Q=-\int_0^A\left(\lambda\frac{\partial T}{dr}\right)dA=\int_0^A\bar{h}(T_\text{w}-T_\text{f})dA \tag{25}$$

where $\bar{h}$ is the area-weighted average wall function heat transfer coefficient for isothermal source or sink

$$\bar{h}=\frac{\int_0^A hdA}{\int_0^A dA} \tag{26}$$

Modified Rayleigh number (Ra_m) is defined as

$$\text{Ra}_\text{m}=\text{Gr}_\text{m}\times\text{Pr}=\frac{\beta g\rho^2d^3QH_0}{A\mu^2\lambda} \tag{27}$$

where Pr is the Prandtl number.

Rayleigh number is defined as

$$\text{Ra}=\text{Gr}\times\text{Pr}=\frac{\beta gc_\text{p}\rho^2L_\text{c}^3\delta T}{\mu\lambda} \tag{28}$$

where L_c is the characteristic length and δT is the temperature difference between fluid and wall.

All properties are calculated at the bulk mean temperature (T_m) of the loop fluid, defined as

$$T_\text{m}=\frac{\sum_{i=1}^{n}T_i}{n} \tag{29}$$

where n is the number of cross sections considered in the loop.

Average temperature of the loop is defined as

$$T_{\text{avg}}=\frac{T_\text{C}+T_\text{H}}{2} \tag{30}$$

where T_C and T_H are the isothermal wall temperatures of sink and source, respectively.

For wall conduction

$$\nabla^2T=0 \tag{31}$$

Boundary conditions

(i) No-slip and no-penetration boundary conditions are applied near the walls.
(ii) All external walls except source and sink are perfectly insulated.
(iii) For internal walls, conjugate heat transfer is considered.
(iv) Source and sink wall temperatures are known boundary conditions.

2.2.2 Simulation Details. A 3D geometry was prepared and steady-state simulation was carried out, where the implicit-coupled finite-volume method was used to discretize the governing equations. The *pressure-implicit with splitting of operators* algorithm was used to solve the coupling model between velocity and pressure.

The momentum and energy terms in the governing equations are iterated with a second-order upwind scheme that uses the upstream values and gradients to compute the control volume face values. Turbulence parameters (k, ε, etc.) are also iterated with a second-order upwind scheme. The *pressure staggering option* scheme is used to discretize the pressure term. No-slip boundary condition is used on the pipe walls. For the near wall treatment, a standard wall function has been assumed in case of turbulent flow [26]. This function has been also used successfully in previously reported relevant studies [12,27]. Axial conduction and viscous dissipation in fluid are considered, while axial conduction along the tube wall is incorporated as well. Convergence is obtained when various residuals of the parameters (temperature, velocity, pressure, etc.) change with the iterations within a preset convergence criterion of 10^{-3} for the residuals of continuity equation

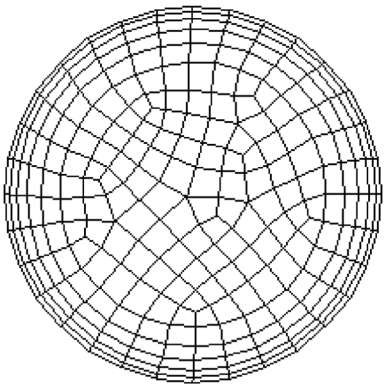

Fig. 2 Meshing of a cross section (fluid part only)

and 10^{-6} for the energy equation. Conservation of mass and energy is also checked for all the cases in the analysis.

Figure 2 shows the meshing of a cross section (fluid part only) of the loop which has a minimum grid size of 0.2 mm in radial direction near the wall and increases to the maximum grid size of 1.5 mm away from the wall. Coarse meshing is adopted in the axial direction (5 mm grid size in horizontal pipes including bends and 10 mm for vertical pipes). Mesh generation yielded a total of 235,552 nodes. The values of nondimensional parameters Y^+ and Y^* have been checked for all the cases of turbulent flow to ensure optimal choice of fineness of grid. The maximum Y^+ and Y^* values in the present study are 54.5 and 54.4, respectively, which ensure that the grid is suitable for the assumption of standard wall function near the wall [26]. Grid independence tests were carried out and results with fine and coarse grids were compared (Table 2). In case of fine grid, 0.1 mm grid size was considered near the wall and 0.4 mm away from the wall; in case of coarse grid, a 0.3 mm grid size was considered near the wall and 1.2 mm away from the wall. Results are obtained for a loop operating pressure of 90 bar with source and sink temperatures of 323 K and 305 K, respectively. Performance of the loop is presented in terms of mass flow rate (m) and heat transfer rate (Q). It may be noted that the differences between coarse and fine grid results are within 1%.

Parameters Y^+ and Y^* are defined as

$$Y^+ \equiv \rho u_\tau y/\mu \tag{32}$$

where u_τ is the friction velocity, defined as $\sqrt{(\tau_w/\rho)}$, in which τ_w is the wall shear stress

$$Y^* \equiv \frac{\rho C_\mu^{1/4} k_t^{1/2} y}{\mu} \tag{33}$$

where k_t is the turbulent kinetic energy, y is the distance from the wall, and $C_\mu = 0.0845$.

2.3 Calculation of Thermophysical Properties of CO_2. Since the state of CO_2 inside the loop varies from subcritical to supercritical and the variation in thermophysical properties near the critical point is extremely large, it is essential to adequately capture the property variation due to changes in temperature. However, as shown in the literature, due to very small variation in operating pressure throughout the NCL (occurs due to very low viscosity of CO_2), the effect of variation of pressure on the properties of single-phase CO_2 is not expected to be significant [18,28,29]. For example, in the present study, the maximum pressure drop in the entire loop is 0.06 bar (±0.03 bar) at operating pressure of 100 bar, which is equal to ±0.03% of the average operating pressure. Hence, for a given operating pressure, the properties of CO_2 at any point in the loop are calculated at the fixed operating pressure and local temperature. The required properties of CO_2 including density, specific heat, thermal conductivity, and viscosity are obtained from the NIST Standard Reference Database REFPROP Version 9.1 [30]. The properties of CO_2 for the operating temperature range at a temperature difference of 1 K are added to the fluid properties library, and a piecewise-linear interpolation approach is used to calculate the properties within the same temperature difference.

Table 2 Grid independence test for operating pressure 90 bar and sink and source temperatures 305 K and 323 K, respectively

Minimum grid size (mm)	No. of nodes	Heat transfer rate (W)	Mass flow rate (kg/s)
0.1	387,000	2239	0.07932
0.2	235,552	2217	0.07803
0.3	140,085	2174	0.07569

3 Results and Discussion

This study has been carried out for a wide range of operating pressures and temperatures of NCL. The operating temperature range is chosen such that it covers the subcritical and supercritical region of CO_2 and would be useful for various engineering applications of heat transfer. Operating pressure of the loop is defined at the center of the isothermal source.

3.1 Heat Transfer Rate of Subcritical and Supercritical CO_2. Heat transfer rate of subcritical liquid and supercritical CO_2 is shown in Figs. 3(*a*) and 3(*b*), respectively. Results are obtained for different ΔT (temperature difference between isothermal source and sink) at various average temperatures of the NCL. Operating average temperature for Fig. 3(*a*) is 283 K which is relevant in air conditioning applications. The operating pressure choice ensures that CO_2 remains in liquid phase only (Fig. 3(*a*)). Results also show that in the subcritical region, a lower operating pressure of liquid CO_2 leads to a higher heat transfer rate. This may be attributed to the variation of thermophysical properties of liquid CO_2 with pressure such that operation of the loop near the saturation point yields better performance. At constant pressure, as liquid temperature approaches saturation temperature, its volumetric expansion coefficient and specific heat increase, whereas viscosity decreases. The changes in these properties are favorable in an NCL, which lead to increase in heat transfer rate.

For the supercritical region, studies are carried out at an operating average temperature of 313 K shown in Fig. 3(*b*) to obtain typical heat transfer behavior of supercritical CO_2. Figure 3(*b*) shows that the heat transfer rate is the highest for an operating pressure of 90 bar. Average operating temperature (313 K) of the loop is close to the pseudocritical point (313.2 K) at 90 bar which causes higher heat transfer rate at this pressure. From thermodynamic properties data [30], pseudocritical points for various operating pressures of CO_2 have been obtained and shown in Table 3. Results have also been obtained for average operating temperatures of 323 K and 333 K and shown in Figs. 3(*c*) and 3(*d*), respectively. The results exhibit that near the pseudocritical region, supercritical fluid yields higher heat transfer rate due to favorable thermophysical properties. As operating temperature increases, pseudocritical region shifts toward higher pressure (Table 3).

3.2 Optimum Operating Condition for Maximum Heat Transfer Rate. Optimum operating condition is defined here as the operating pressure at which heat transfer rate is the maximum for a given average operating temperature of the loop. Based on the studies carried out for subcritical and supercritical fluid based NCLs, it can be concluded that the optimum operating condition

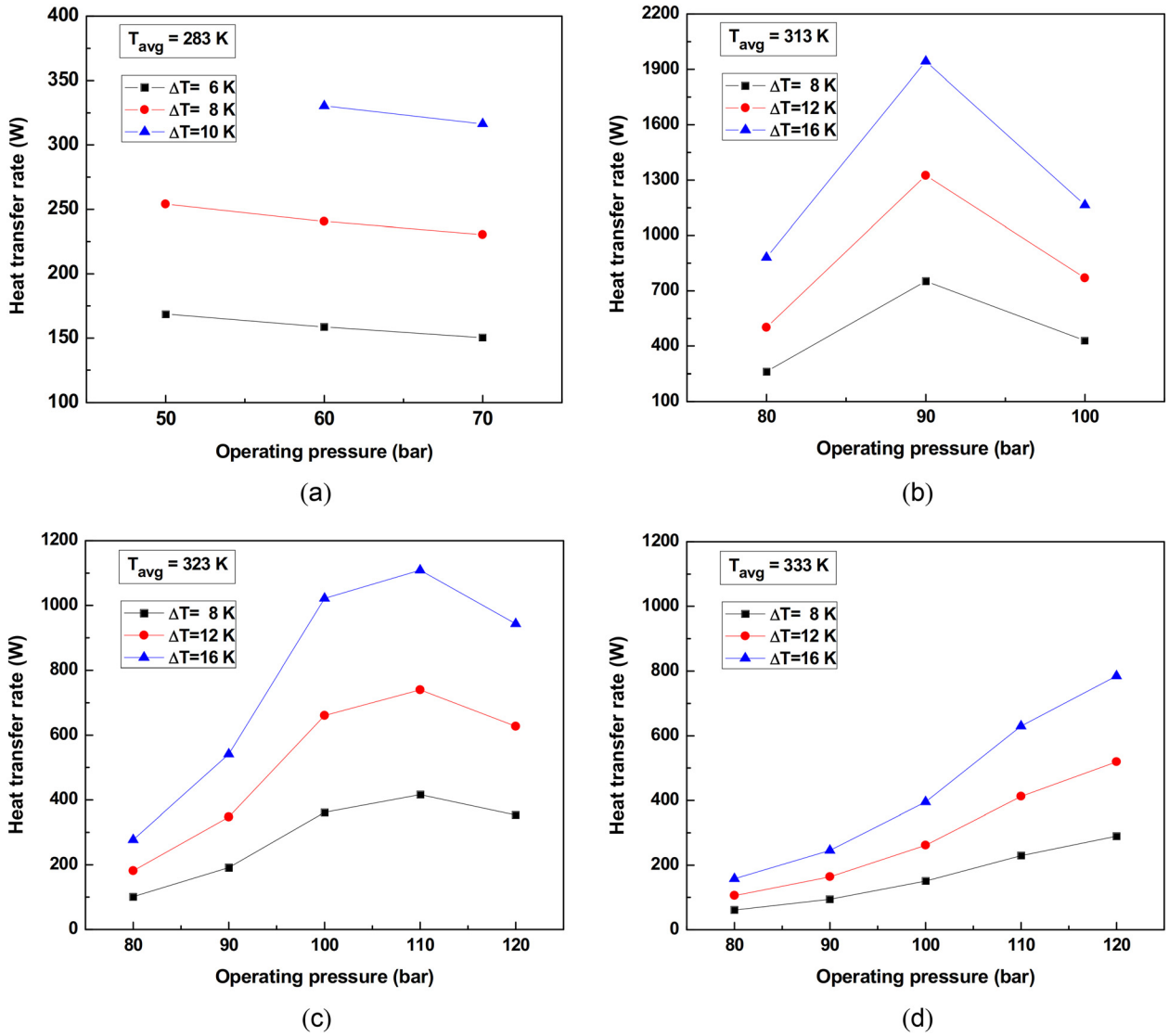

Fig. 3 Variation in heat transfer rate with ΔT for (*a*) subcritical CO_2, (*b*) supercritical CO_2 at 313 K, (*c*) supercritical CO_2 at 323 K, and (*d*) supercritical CO_2 at 333 K

for subcritical fluid (for liquid phase) lies near the saturation pressure for a given average operating temperature of the loop. For supercritical fluid, studies have been carried out and correlations have been proposed for quick estimation of optimum operating condition. Different criteria are used to obtain distinct correlations for optimum pressure at given operating temperature of the loop as shown below.

- Correlation based on pseudocritical point (c_{p_max})
- Correlation based on Rayleigh number (Ra)
- Correlation based on modified Rayleigh number (Ra_m)

Table 3 Pseudocritical point for various operating pressures of CO_2

Pressure (bar)	Pseudocritical point (K)
80	307.8
90	313.2
100	318.1
110	322.8
120	327.2

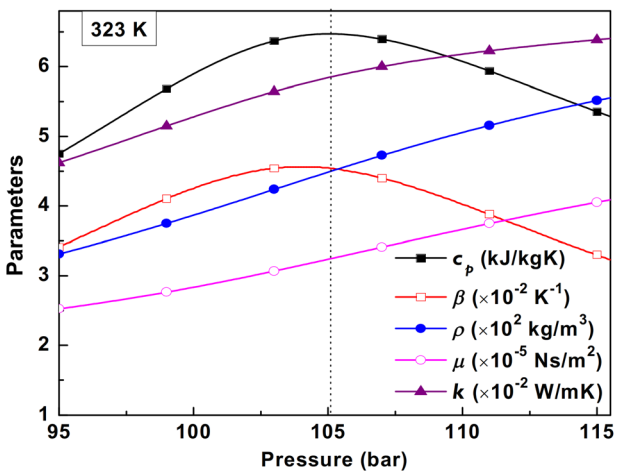

Fig. 4 Variation of thermophysical properties with pressure

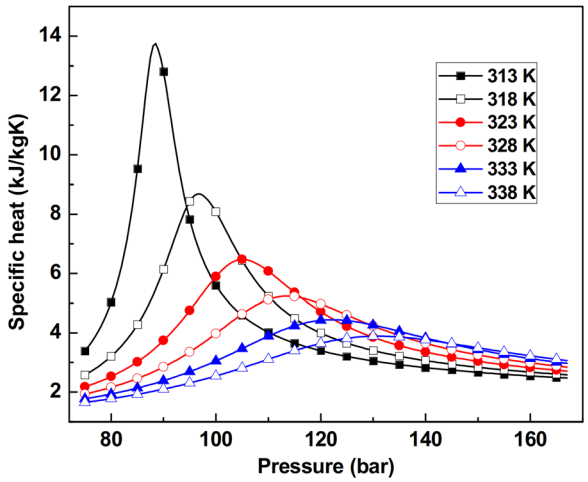

Fig. 5 Variation of specific heat of CO_2 with pressure for different temperatures

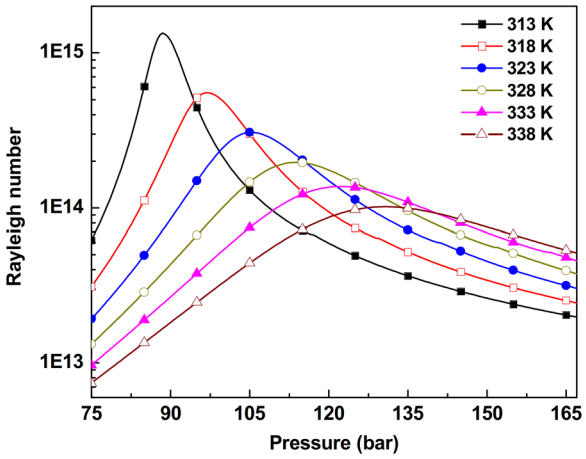

Fig. 7 Variation of Rayleigh number with pressure for different operating temperatures

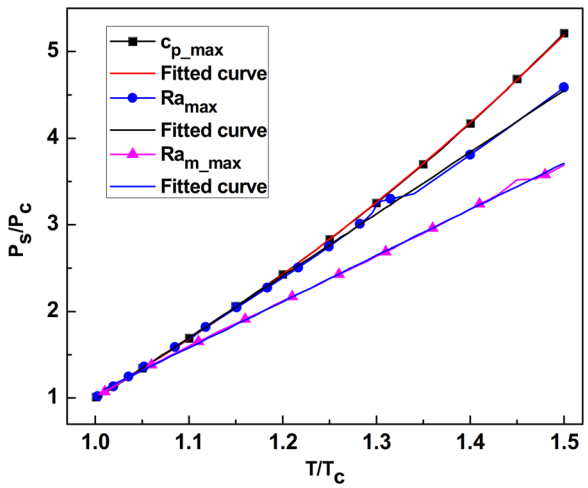

Fig. 6 Variation of optimum pressure of CO_2 with temperature

In general, for efficient heat transfer, pseudocritical point is chosen as optimum operating condition for forced as well as for NCLs. As explained before, for natural convection or NCLs, other properties like volumetric expansion coefficient also play an important role in addition to specific heat. Figure 4 indicates that the peak of specific heat does not occur exactly where the peak of volumetric expansion coefficient occurs. It will be more meaningful to define optimum operating condition for natural convection based on Rayleigh number which takes care of variation of all the relevant thermophysical properties. Many authors have defined modified Grashof number for the heat transfer studies of NCL. Based on modified Grashof number, modified Rayleigh number has been defined. Correlation has also been developed based on modified Rayleigh number (Ra_m) and compared with other two correlations for maximum heat transfer rate.

3.2.1 Correlation Based on Pseudocritical Point (c_{p_max}). Figure 5 shows the variation of specific heat for different operating temperatures of CO_2 with pressure. Peaks of specific heat for different operating temperature represent pseudocritical points. Based on the peak value of specific heat at different operating temperatures, a correlation is obtained for optimum operating pressure. Figure 6 shows the variation of optimum pressure with temperature for supercritical CO_2 based on c_{p_max}, Ra_{max}, and Ra_{m_max}. Correlations are expressed generically in terms of the reduced pressure and temperature so that they can be applied universally to other fluids as well. The correlation obtained based on pseudocritical points is also validated with fluids other than CO_2 (Table 4).

Correlation based on c_{p_max}

$$\frac{P_s}{P_c} = -0.724443 - 2.63722\left(\frac{T}{T_c}\right) + 4.38658\left(\frac{T}{T_c}\right)^2 \quad (1.0 \le T/T_c \le 1.5) \tag{34}$$

where P_s and P_c are the pseudocritical pressure (optimum pressure) and critical pressure of the fluid, respectively.

The proposed correlation exhibits a R^2 value of 99.99% reflecting excellent regressed fit with the actual data. Results also reveal that the proposed correlation yields a maximum difference of less than 5% with the actual data which is quite reasonable.

3.2.2 Correlation Based on Rayleigh Number (Ra_{max}). Rayleigh number is defined as

$$\mathrm{Ra} = \mathrm{Gr} \times \mathrm{Pr} = \frac{\beta g c_p \rho^2 L_c^3 \delta T}{\mu k} \tag{35}$$

Table 4 Validation of pressure correlation based on pseudocritical point for given temperature with other fluids (based on c_{p_max})

Fluids	T_c (K)	P_c (bar)	T/T_c	P_s/P_c (theoretical)	P_s/P_c (correlation)	Error (%)
CO_2	304.13	73.77	1.1	1.69	1.682	0.6
Water	647.1	220.6	1.1	1.77	1.682	4.7
Ammonia	405.4	113.3	1.1	1.70	1.682	1.0
Propane	369.9	42.48	1.1	1.67	1.682	0.7
R134a	374.2	40.59	1.1	1.75	1.682	3.8
N_2O	309.52	72.45	1.1	1.66	1.682	1.6

Table 5 Validation of pressure correlation based on Rayleigh number for given temperature with other fluids (based on Ra_{max})

Fluids	T/T_c	P_s/P_c (theoretical)	P_s/P_c (correlation)	Error (%)
CO_2	1.1	1.69	1.70	0.3
Water	1.1	1.79	1.70	5.2
Ammonia	1.1	1.70	1.70	0.5
Propane	1.1	1.68	1.70	0.9
R134a	1.1	1.74	1.70	2.7
N_2O	1.1	1.67	1.70	1.6

Table 6 Validation of pressure correlation based on modified Rayleigh number for given temperature with other fluids (based on Ra_{m_max})

Fluids	T/T_c	P_s/P_c (theoretical)	P_s/P_c (correlation)	Error (%)
CO_2	1.1	1.60	1.58	1.4
Water	1.1	1.74	1.58	9.2
Ammonia	1.1	1.64	1.58	3.7
Propane	1.1	1.61	1.58	1.6
R134a	1.1	1.65	1.58	4.3
N_2O	1.1	1.49	1.58	6.3

where the characteristic length (L_c) and temperature difference between fluid and wall (δT) are assumed to be unity.

Figure 7 shows the variation of Rayleigh number with pressure for different temperatures of CO_2. Based on the peaks of Rayleigh number (Ra_{max}), correlation has been developed for optimum pressure (P_s). Figure 6 shows the variation of optimum pressure with temperature for supercritical CO_2 based on Ra_{max}.

Correlation based on Rayleigh number

$$\frac{P_s}{P_c} = -6.15846 + 7.14089\left(\frac{T}{T_c}\right) \quad (1.0 \le T/T_c \le 1.5) \tag{36}$$

The proposed correlation exhibits a R^2 value of 99.92% reflecting excellent regressed fit with the actual data. Results show that the proposed correlation yields a modest maximum difference of 5.2% with the actual data. The correlation obtained based on Rayleigh number is also validated with fluids other than CO_2 (Table 5).

3.2.3 Correlation Based on Modified Rayleigh Number (Ra_{m_max}). Modified Rayleigh number (Ra_m) is defined as

$$Ra_m = Gr_m \times Pr = \frac{\beta g \rho^2 d^3 Q H_0}{A \mu^2 k} \tag{37}$$

where $d = 1$ cm, $H_0 = 1$ m, and $Q = 100$ W are considered for developing the correlation. Any constant values can be assigned to these parameters. Different constant values will affect the magnitude of Ra_m but pressure of peak point will not change.

Figure 8 shows the variation of modified Rayleigh number with pressure for different temperatures of CO_2. Based on the peaks of modified Rayleigh number (Ra_{m_max}), a correlation has been developed for the optimum pressure (P_s). Figure 6 depicts variation of optimum pressure with temperature for supercritical CO_2 based on Ra_{m_max}.

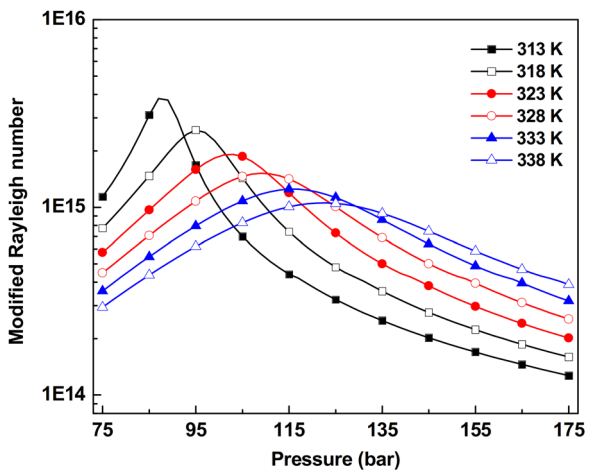

Fig. 8 Variation of modified Rayleigh number with pressure for various operating temperatures

Correlation based on modified Rayleigh number

$$\frac{P_s}{P_c} = -4.26611 + 5.31627\left(\frac{T}{T_c}\right) \quad (1.0 \le T/T_c \le 1.5) \tag{38}$$

The proposed correlation exhibits an R^2 value of 99.94% reflecting excellent regressed fit with the actual data. Results show that the proposed correlation yields a maximum difference of 9.2% with the actual data. The correlation obtained based on modified Rayleigh number is also validated with several fluids other than CO_2 (Table 6).

3.3 Comparison Among the Developed Correlations in Terms of Heat Transfer Rate. All the above-mentioned correlations for optimum operating conditions for supercritical NCLs are compared in terms of heat transfer rate. Figure 9(*a*) shows that the optimum condition obtained employing correlation based on Rayleigh number yields the highest heat transfer rate. Heat transfer rate is calculated employing CFD simulation for the above-mentioned NCL with isothermal source and sink. Results show that the optimum pressure based on modified Rayleigh number is much lower with low heat transfer rate, whereas optimum pressure based on Rayleigh number is highest with maximum heat transfer rate.

For maximum heat transfer rate, correlation based on Rayleigh number is also checked for different operating pressures and is shown in Fig. 9(*b*). Results are obtained for two different pressures on either side of the computed optimum pressure (±5 bar). It is seen that the heat transfer rate is indeed highest at the operating pressure calculated based on the Rayleigh number correlation. It is concluded that correlation based on Rayleigh number should be used to estimate the optimum operating pressure for higher heat transfer rate in NCLs.

3.4 Validation of Obtained Results With Published Experimental Data. In order to validate the results obtained from the CFD simulation, an additional comparison was carried out employing the experimental data reported earlier by Vijayan [31]. The comparison was made in terms of nondimensional parameters Reynolds number (Re) and modified Grashof number (Gr_m), which are calculated at the bulk mean temperature (T_m) of the loop. Figure 10 shows that even though the data trends agree reasonably well, significant quantitative difference exists between the present prediction and the previously reported measured data. This may be attributed to the geometric dissimilarity in the two studies and experimental uncertainty.

Vijayan correlation [31]

$$Re = 1.96(Gr_m d/L_t)^{\frac{1}{2.75}} \tag{39}$$

(turbulent flow).

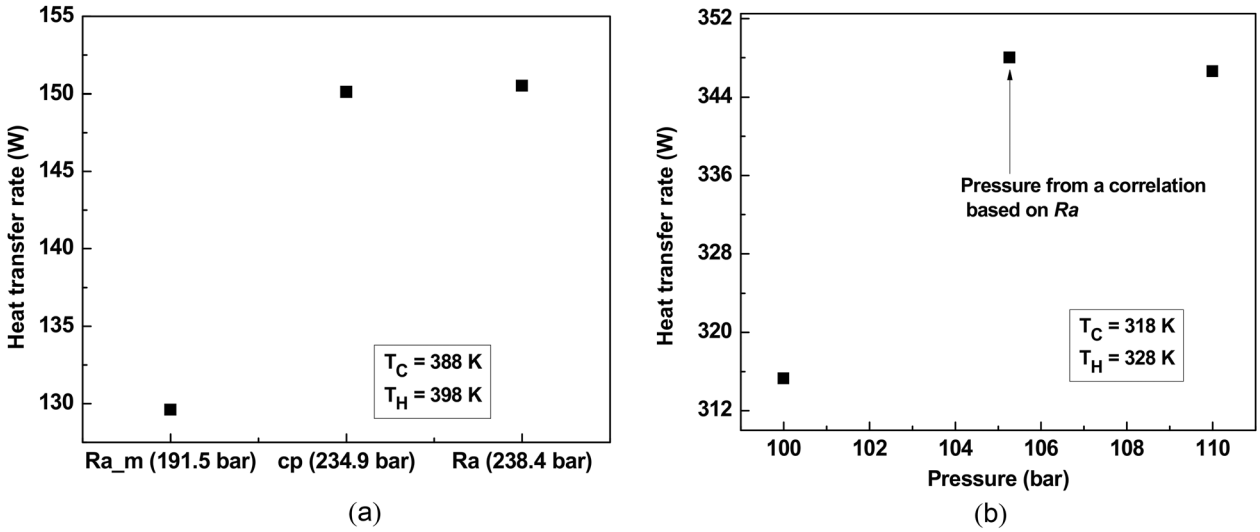

Fig. 9 (*a*) Comparison of developed correlations in terms of heat transfer rate and (*b*) variation of heat transfer rate near the obtained pressure employing correlation based on Rayleigh number

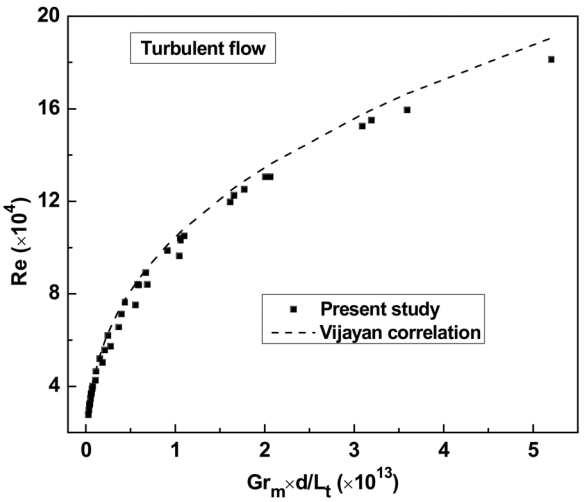

Fig. 10 Validation of obtained result with experimental data for turbulent flow

4 Conclusions

This study presents 3D CFD analyses to obtain the optimum operating conditions based on maximum heat transfer rate for subcritical and supercritical CO_2-based NCLs. The following inferences are made:

(i) For a given loop geometry, supercritical CO_2 yields higher heat transfer rate (if operated near pseudocritical region) than subcritical (liquid/vapor) CO_2.
(ii) For subcritical liquid phase, the optimum operating condition occurs near the saturation pressure at a given average operating temperature of the loop.
(iii) Three correlations are proposed for supercritical fluids to obtain optimum operating condition. Correlation based on Rayleigh number is found to yield higher heat transfer rate. These correlations are presented generically in terms of reduced temperature and reduced pressure so that they can be employed for a wide variety of fluids operating in the supercritical region. Correlations are also validated with different loop fluids.

These results are expected to help design superior optimal NCLs for critical applications.

Nomenclature

A = area
c_p = specific heat capacity
C_v = constant
C_μ, $C_{1\varepsilon}$, $C_{2\varepsilon}$, $C_{3\varepsilon}$ = parameters in RNG model equations
d = diameter of inner pipe or loop diameter
E = energy
g = gravitational acceleration
G_b = turbulent kinetic energy due to buoyancy
G_k = turbulent kinetic energy due to mean velocity gradient
Gr = Grashof number
Gr_m = modified Grashof number
h = heat transfer coefficient
H_0 = total height of vertical pipes
k = turbulent kinetic energy
L = length of isothermal source/sink
L_c = characteristic length
L_t = total length of the loop
L_0 = total length of a horizontal pipe
L_1 = adiabatic pipe length on horizontal pipe
m = mass flow rate
p, P = pressure of fluid
Pr = Prandtl number
Pr_t = turbulent Prandtl number
Q = heat transfer rate
r = radius of loop
R = radius of curvature for bends
R_ε = parameters in RNG model equations
Ra = Rayleigh number
Re = Reynolds number
S = strain tensor
T = temperature
u, v, V = velocity
x = x-coordinate location
y = distance from the wall
Y^+, Y = nondimensional number

Greek Symbols

α, α_0 = thermal diffusivity
α_k, α_ε = parameters in RNG model equations
β = volumetric expansion coefficient
ΔT = temperature difference across the CHX/HHX

δT = temperature difference between fluid and wall
ε = turbulence dissipation rate
η = parameter in RNG model
λ = thermal conductivity
μ = dynamic viscosity
μ_t, μ_{eff} = viscosity parameters in RNG model
ρ = density of fluid
$\bar{\bar{\tau}}$ = stress tensor
τ_w = wall shear stress

Subscripts

avg = average
c = critical
C = sink
CO_2 = carbon dioxide
eff = effective
f = fluid
H = source
i = x-direction/internal
j = y-direction
m = modified, bulk mean
r = radial direction
ref = reference
s = optimum
w = wall
z = axial direction
θ = azimuthal direction

References

[1] Wang, K., Magnus, E., Yunho, H., and Radermacher, R., 2010, "Review of Secondary Loop Refrigeration System," Int. J. Refrig., **33**(2), pp. 212–234.
[2] Kumar, K. K., and Ram Gopal, M., 2009, "Carbon Dioxide as Secondary Fluid in Natural Circulation Loops," Proc. Inst. Mech. Eng., Part E, **223**(3), pp. 189–194.
[3] Yadav, A. K., Bhattacharyya, S., and Ram Gopal, M., 2014, "On the Suitability of Carbon Dioxide in Forced Circulation Type Secondary Loops," Int. J. Low Carbon Technol., **9**(1), pp. 85–90.
[4] Kreitlow, D. B., and Reistad, G. M., 1978, "Thermosyphon Models for Downhole Heat Exchanger Application in Shallow Geothermal Systems," ASME J. Heat Transfer, **100**(4), pp. 713–719.
[5] Torrance, K. E., 1979, "Open-Loop Thermosyphons With Geological Application," ASME J. Heat Transfer, **100**(4), pp. 677–683.
[6] Rieberer, R., 2005, "Naturally Circulation Probes and Collectors for Ground-Coupled Heat Pumps," Int. J. Refrig., **28**(8), pp. 1308–1315.
[7] Zhang, X. R., and Yamaguchi, H., 2007, "An Experimental Study on Evacuated Tube Solar Collector Using Supercritical CO_2," Appl. Therm. Eng., **28**(10), pp. 1225–1233.
[8] Zimmermann, A. J. P., and Melo, C., 2014, "Analysis of a R744 Two Phase Loop Thermosyphon Applied to the Cold End of a Stirling Cooler," Appl. Therm. Eng., **73**(1), pp. 549–558.
[9] Rieberer, R., Karl, M., and Hermann, H., 2004, "CO_2 Two-Phase Thermosyphon as a Heat Source System for Heat Pumps," 6th IIR-Gustav Lorentzen Natural Working Fluids Conference, Glasgow, UK, Aug. 29–Sept. 1 pp. 1–8.
[10] Ochsner, K., 2008, "Carbon Dioxide Heat Pipe in Conjunction With a Ground Source Heat Pump (GSHP)," Appl. Therm. Eng., **28**(16), pp. 2077–2082.
[11] Sarkar, M. K. S., Tilak, A. K., and Basu, D. N., 2014, "A State-of-the-Art Review of Recent Advances in Supercritical Natural Circulation Loops for Nuclear Applications," Ann. Nucl. Energy, **73**, pp. 250–263.
[12] Yadav, A. K., Ram Gopal, M., and Bhattacharyya, S., 2012, "CO_2 Based Natural Circulation Loops: New Correlations for Friction and Heat Transfer," Int. J. Heat Mass Transfer, **55**(17–18), pp. 4621–4630.
[13] Sabersky, R. H., and Hauptmann, E. G., 1967, "Forced Convection Heat Transfer to Carbon Dioxide Near the Critical Point," Int. J. Heat Mass Transfer, **10**(11), pp. 1499–1508.
[14] Yamagata, K., Nishmawa, K., Hasegawa, T. S., Fuji, T., and Yoshida, M. S., 1972, "Forced Convective Heat Transfer to Supercritical Water Flowing in Tubes," Int. J. Heat Mass Transfer, **15**(12), pp. 2575–2593.
[15] He, S., Kim, W. S., and Jackson, J. D., 2008, "A Computational Study of Convective Heat Transfer to Carbon Dioxide at a Pressure Just Above the Critical Value," Appl. Therm. Eng., **28**(13), pp. 1662–1675.
[16] Hua, Y. X., Wang, Y. Z., and Meng, H., 2010, "A Numerical Study of Supercritical Forced Convective Heat Transfer of n-Heptane Inside a Horizontal Miniature Tube," J. Supercrit. Fluids, **52**(1), pp. 36–46.
[17] Du, Z., Lin, W., and Gu, A., 2010, "Numerical Investigation of Cooling Heat Transfer to Supercritical CO_2 in a Horizontal Circular Tube," J. Supercrit. Fluids, **55**(1), pp. 116–121.
[18] Yadav, A. K., Ram Gopal, M., and Bhattacharyya, S., 2012, "CFD Analysis of a CO_2 Based Natural Circulation Loop With End Heat Exchangers," Appl. Therm. Eng., **36**, pp. 288–295.
[19] Yoshikawa, S., Smith, R. L., Jr., Inomata, H., Matsumura, Y., and Arai, K., 2005, "Performance of a Natural Convection Circulation System for Supercritical Fluids," J. Supercrit. Fluids, **36**(1), pp. 70–80.
[20] Seetharam, T. R., and Sharma, G. K., 1979, "Free Convective Heat Transfer to Fluids in the Near-Critical Region From Vertical Surfaces With Uniform Heat Flux," Int. J. Heat Mass Transfer, **22**(1), pp. 13–20.
[21] Liao, S. M., and Zhao, T. S., 2002, "Measurements of Heat Transfer Coefficients From Supercritical Carbon Dioxide Flowing in Horizontal Mini/Micro Channels," ASME J. Heat Transfer, **124**(3), pp. 413–420.
[22] Yamamoto, S., Furusawa, T., and Matsuzawa, T., 2011, "Numerical Simulation of Supercritical Carbon Dioxide Flows Across Critical Point," Int. J. Heat Mass Transfer, **54**(4), pp. 774–782.
[23] Yang, J., Oka, Y., Ishiwatari, Y., Liu, J., and Yoo, J., 2007, "Numerical Investigation of Heat Transfer in Upward Flow of Supercritical Water in Circular Tubes and Tight Fuel Rod Bundles," Nucl. Eng. Des., **237**(4), pp. 420–430.
[24] Lisboa, P. F., Fernandes, J., Simoes, P. C., Mota, J. P. B., and Saatdjian, E., 2010, "Computational-Fluid-Dynamics Study of a Kenics Static Mixer as a Heat Exchanger for Supercritical Carbon Dioxide," J. Supercrit. Fluids, **55**(1), pp. 107–115.
[25] Vijayan, P. K., and Austregesilo, H., 1994, "Scaling Laws for Single-Phase Natural Circulation Loops," Nucl. Eng. Des., **152**(1–3), pp. 331–347.
[26] Launder, B. E., and Spalding, D. B., 1974, "The Numerical Computation of Turbulent Flows," Comput. Methods Appl. Mech. Eng., **3**(2), pp. 269–289.
[27] Yadav, A. K., Ram Gopal, M., and Bhattacharyya, S., 2014, "Transient Analysis of Subcritical/Supercritical Carbon Dioxide Based Natural Circulation Loops With End Heat Exchangers: Numerical Studies," Int. J. Heat Mass Transfer, **59**, pp. 24–33.
[28] Kumar, K. K., and Ram Gopal, M., 2009, "Steady-State Analysis of CO_2 Based Natural Circulation Loops With End Heat Exchangers," Appl. Therm. Eng., **29**(10), pp. 1893–1903.
[29] Zhang, X., Chen, L., and Yamaguchi, H., 2010, "Natural Convective Flow and Heat Transfer of Supercritical CO_2 in a Rectangular Circulation Loop," Int. J. Heat Mass Transfer, **53**(19–20), pp. 4112–4122.
[30] NIST, 2013, Standard Reference Database-REFPROP, Version 9.1, National Institute of Standards and Technology, Gaithersburg, MD.
[31] Vijayan, P. K., 2002, "Experimental Observations on the General Trends of the Steady State and Stability Behaviour of Single-Phase Natural Circulation Loops," Nucl. Eng. Des., **215**(1–2), pp. 139–152.